APPLICATION OF MICRO FRESNEL LENSES IN OUTPUT ENHANCEMENT OF SOLAR CELLS

NURA LIMAN CHIROMAWA

UNIVERSITI SAINS MALAYSIA

2016

APPLICATION OF MICRO FRESNEL LENSES IN OUTPUT ENHANCEMENT OF SOLAR CELLS

by

NURA LIMAN CHIROMAWA

Thesis submitted in fulfillment of the requirements for the degree of Doctor of Philosophy

March, 2016

ACKNOWLEDGEMENT

Praise is to ALLAH, HIS bounties and bliss is on HIS messenger (Prophet Muhammad peace be upon him) and his household, his companions and on all who follow the guidance until the day of Judgment.

I wish to tender my profound gratitude to my main supervisor in person of **Professor, Dr. Alhaj Kamarulazizi Bin Ibrahim** for the guidance, encouragements, and constructive criticisms as well as the supports with relevant materials in the cause of undertaking this research work without whom most of the works in this research work could not have been done. May God almighty be with him and overlook his shortcomings in his present and future life. Ameen.

I also wish to take this unique opportunity to express my appreciation to the School of Physics, Universiti Sains Malaysia for providing me the necessary facilities, an excellent academic environment for a successful completion of my work and also Research Grant for supporting this research work (203/PSF/6721001). Special regards to the technical staffs of Nano-Optoelectronics Research and Technology Laboratory (NOR- Lab) School of Physics Universiti Sains Malaysia for their technical assistances given to me during the experimental activities at the experimental section of the research work. I wish them God's guidance in their future endeavors.

My appreciation also goes to the management of Umaru Musa Yar'adua University, Katsina (UMYUK) in collaborations with the Nigerian Tertiary Education Trust Fund (TET-Fund) for the financial sponsorship leading to the success of this research work.

Gratitude, thankfulness, and prosperity to my father late *Mallam Liman Chiromawa* (may his soul rest in perfect peace) and his family especially my beloved mother *Hajiya Hafsat Ibrahim,* for their supports, guidance, and assistances leading to the progressive success in all my endeavors right from when, and before I was born. May God Almighty reward them "JANNATUL FIRDAUSI", Ameen. Finally, to my family for been with me through all these years of academic struggles and for their patience and endurance. I wish them God's guidance in their future endeavors.

NURA LIMAN CHIROMAWA

MARCH, 2016

TABLE OF CONTENTS **Page**

Acknowledgement……..ii

Table of Contents……....iv

List of Tables……...x

List of Figures……xi

List of Abbreviations……xix

List of Symbols……..xxi

Abstrak ……xxiv

Abstract ……... xxvi

CHAPTER 1 – INTRODUCTION …….1

1.1 Overview……1

1.2 Motivations and problem statements…….……2

1.3 Objectives of the research……...4

1.4 Research originality...…….5

1.5 Scope of thesis ……...5

1.6 Outline of the thesis……6

CHAPTER 2 - LITERATURE REVIEW…….7

2.1 Introduction……7

2.2 Concentrator PV systems ……..7

2.3 Fresnel lens CPV system……..…… 10

CHAPTER 3 - PRINCIPLES OF FRESNEL LENSES CPV-SYSTEM, SOLAR CELLS AND MICRO/NANO FABRICATION IN OPTICAL APPLICATIONS ……18

3.1 Introduction …….....18

3.2 Principles of Fresnel lenses CPV-system …….….18

3.2.1 Performance estimation of Fresnel lenses array CPV-system …… 24

3.3 Crystalline silicon…….. 26

3.3.1 Doping…… ……..27

3.3.2 P-N junction under illumination……29

3.3.3 Characteristics parameters of Solar cells …….30

3.3.4 Ideal Solar cells ……31

3.3.5 Loses on Solar cells ……..33

3.3.6 Actual Solar cells……. 35

3.3.7 Photocurrent and Spectral response ……..36

3.3.8 Effects of temperature on Silicon Solar cells ……..37

3.4 Lens materials…… 38

3.4.1 General properties of optical materials…… 39

3.4.2 Fresnel lens ……...…40

3.5 Principles of Micro and Nano fabrications…….42

3.5.1 Importance of Macro/Nano fabrication in electronics applications … 42

3.5.2 Pattern definition …….43

3.5.3 Pattern transfer ……45

3.5.4 Dry etching technique ……..45

3.5.5 Reactive ion etching RIE ……46

3.5.6 Lift off process ……48

3.5.7 Electron beam resists……49

3.6 PDMS Repilca Molding……50

3.6.1 PDMS Surface chemistry …….....51

3.7 Poly (methyl methacrylate) PMMA …… 53

CHAPTER 4 – METHODOLOGY……55

4.1 Introduction ……... 55

4.2 Sample preparation ……56

4.2.1 Cutting the Wafer …… 56

4.2.2 Wafer Cleaning …… 56

4.2.3 Spin-Coating …… 58

4.3 Pattern generation (EBL) ……60

4.3.1 Fresnel rings design..…… 62

4.3.2 Exposure Parameters.…… 63

4.3.3 Step-size..…….. 63

4.3.4 Dwell-time ....……....64

4.3.5 Beam Current ...…….64

4.3.6 Area Dose……..64

4.3.7 Apertures...……65

4.4 Pattern Development ……65

4.5 Metal deposition techniques ……..67

4.6 Reactive Ion Etching (RIE) Set-up ……67

4.6.1 RIE Parameters ...……..70

4.7 Characterization Equipment ……... 70

4.7.1 Field emission scanning electron microscope (FESEM) ……...70

4.7.2 Energy dispersive x-ray spectroscopy (EDS/EDX) ……...72

4.7.3 Atomic Force Microscope (AFM) ……73

4.7.4 Fourier Transform Infrared Spectrometer (FTIR) …… 74

4.7.5 Optical reflector meter (Filmetrics) ……76

4.7.6 UV-VIS-NIR Spectrometer ……78

4.7.7 Optical Microscope ……78

4.7.8 Solar Simulator System-IV ……80

4.8 Fabrication and Characterization of Micro Array Fresnel rings on Si using EBL and RIE processes……..……..81

4.8.1 Fabrication process of Fresnel rings on Si substrate ……..81

4.8.2 Characterization Process of Si-Fresnel rings Array...…….83

4.9 Fabrication and Characterization of SiO_2 Fresnel lens by EBL process……..84

4.9.1 Fabrication process of PMMA Fresnel lens on SiO_2 substrate …….84

4.9.2 Characterization process of SiO_2 Fresnel lens……86

4.10 Fabrication and Characterization of Micro Array of PMMA/SiO_2 Fresnel Lenses by Mold fabrication process for high efficient Si-Solar cells ……86

4.10.1 Fabrication process of Si-Mold (Master Mold) …….87

4.10.2 Fabrication process of PDMS-Mold and PMMA/SiO_2 Fresnel lens.....88

4.10.3 Characterisation Process of PMMA/SiO_2 Fresnel lenses …….89

CHAPTER 5 - RESULTS AND DISCUSSIONS ……..90

5.1 Introduction……....90

5.2 Discussions of results on the fabricated Micro Array Fresnel rings on

Si by EBL and RIE processes……..91

5.2.1 FESEM/EDX Analyses ……91

5.2.2 AFM Analysis ……...95

5.2.3 Geometrical Analysis ……...102

5.2.4 UV-Vis-NIR Analysis ……...106

5.2.5 FTIR and Filmetrics Analysis ……...109

5.2.6 Summary …….. 113

5.3 Discussions of results on fabricated Fresnel lens on SiO_2 by EBL Process…114

5.3.1 FESEM/EDX Analyses …… 114

5.3.2 AFM Analysis …….. 119

5.3.3 Optical Microscope analysis …… 122

5.3.4 Filmetrics Analysis …….. 124

5.3.5 FTIR and UV-Vis-NIR Analysis ……..125

5.3.6 Summary …….. 131

5.4 Discussions of results on the fabricated Micro array of PMMA/SiO_2 Fresnel lenses by Mold fabrication process and on Si-Solar Cells ……132

5.4.1 FESEM/EDX Analyses ……132

5.4.2 AFM Analysis …….. 135

5.4.3 Solar Simulator Analysis on Si-Solar Cells ……..139

5.4.4 Summary……143

CHAPTER 6 - CONCLUSION AND RECOMMENDATIONS FOR FUTURE WORKS……..…….145

6.1 Introduction ……145

6.2 Conclusion.……..145

6.3 Recommendations for future works.……...147

REFERENCES ……148

APPENDIIX A ……157

LIST OF PUBLICATIONS AND CONFERENCES……158

LIST OF TABLES

		Page
Table 3.1:	Designed parameters of Fresnel lens.	22
Table 4.1:	EBL parameters used for fabrication of Fresnel rings on PMMA/Si.	83
Table 4.2:	EBL exposure conditions showing exposure parameters used for the fabrication process of PMMA/SiO_2 Fresnel lens.	86
Table 5.1:	RIE parameters for Si etching using CHF_3/O_2 at 50/50 sccm flow rate.	102
Table 5.2:	Increase in area and perimeter of Fresnel rings with respect to increase in radius.	104
Table 5.3:	UV-Vis-NIR reflection data analysis on Si surface.	107
Table 5.4:	Summary of FTIR absorption results on the surface of PMMA/Si.	113
Table 5.5:	Summary of FTIR reflection results on the surface of PMMA/Si.	113
Table 5.6:	EDX results of PMMA film layer spun coat on SiO_2.	115
Table 5.7:	Errors occurred on fabricated SiO_2-Fresnel lens during EBL process.	117
Table 5.8:	IR-transmission through PMMA/SiO_2 at different PMMA thickness.	126
Table 5.9:	IR-absorption on PMMA/SiO_2 at different PMMA thickness.	127
Table 5.10:	UV-Vis-NIR transmission data analysis for PMMA/SiO_2.	129
Table 5.11:	Effects of PMMA/SiO_2 Fresnel lenses array on characteristics parameters of Si-Solar Cells.	141

LIST OF FIGURES

		Page
Figure 2.1:	Optical design concept of modular Fresnel lenses for solar flux concentration (a) 3-D of concentration optics (b) facet directions of modularly faceted Fresnel lenses.	11
Figure 3.1:	Schematic illustration of PMMA/SiO_2 Fresnel lenses array on Silicon solar cells.	19
Figure 3.2:	Graphical representation of the designed Fresnel rings' radius against number of Fresnel zone Z.	23
Figure 3.3:	The graphical relationship between the designed focal length of Fresnel lens and the wavelength of visible light	23
Figure 3.4:	Schematic illustration of Fresnel lens (a) 2-dimensional view showing the concentric rings of Fresnel lens (b) Side view showing the optical Parameters of Fresnel lens as a concentrator PV system.	24
Figure 3.5:	Crystal structure of Silicon.	27
Figure 3.6:	Doping and concentration distribution of a symmetrical *p-n* junction in thermal equilibrium.	28
Figure 3.7:	Current and Voltage (I-V) characteristics (a) at standard condition (b) under illumination.	29
Figure 3.8:	The circuit arrangement for a solar cell comprising both ideal and real situations.	32
Figure 3.9:	Schematic diagram of typical solar cell losses.	33
Figure 3.10:	Top-down and bottom-up nanofabrication methods.	43
Figure 3.11:	Comparison between different lithographic techniques.	44
Figure 3.12:	Theoretical schematic illustration of typical RIE-reactor (a) and (b) Practical configuration of RIE chamber.	47
Figure 3.13:	The schematic steps of (a) Lift-off process and (b) Plasma etching.	49
Figure 3.14:	Schematic illustration of replica molding method.	51

Figure 3.15:	Chemical and structural formulas of PDMS (a) Chemical formula and (b) 3-Dimensional structure.	52
Figure 3.16:	Chemical and structural formulas of PMMA (a) Chemical formula and (b) 3-Dimensional structure.	54
Figure 4.1:	Flowchart of the fabrication processes of Fresnel lenses for solar photovoltaic concentrator system.	55
Figure 4.2:	Diamond Scriber (Model type; RV129) of the Nano-optoelectronics Research and Technology Laboratory (USM).	56
Figure 4.3:	The schematic diagram of spin coating process, (a) deposition of the photoresist on the substrate, (b) Spin up, (c) Spin off, and (d) drying.	59
Figure 4.4:	The thickness h, against the rotational speed ω of PMMA 950 A2, A4, and A7 for the duration of 90 sec.	60
Figure 4.5:	(a) Electron beam lithography set up, (b) Scanning electron microscopy (SEM) JEOL JSM-6460LV with Raith-ELPHY Quantum for EBL system (NOR, USM).	61
Figure 4.6:	Extended GDSII interface for pattern design.	62
Figure 4.7:	The exposure dialog box in ELPHY Quantum software showing exposure parameters.	63
Figure 4.8:	Schematic of e-beam configuration showing the different concept of dose area, lines and dots.	64
Figure 4.9:	Differences between developed structures from positive and negative photoresists.	66
Figure 4.10:	Schematic of a typical parallel plate Plasma etch system.	68
Figure 4.11:	ICP-RIE system (model: Oxford Plasmalab 80 Plus).	69
Figure 4.12:	The typical FE-SEM (a) Field emission electron gun, (b) FE-SEM image (Model: FEI Nova NanoSEM 450 and Zeiss Supra 35VP).	71
Figure 4.13:	Schematic diagram showing the Energy dispersive x-ray spectroscopy (EDX) set up.	72

Figure 4.14:	Typical set-up of an atomic force microscopy AFM.	73
Figure 4.15:	The schematic illustration of the basics for the working principles of FTIR.	75
Figure 4.16:	Fourier transforms infrared spectrometer (FTIR) system; Model: PERKIN ELMER SPCTRUM GX.	76
Figure 4.17:	(a) Principles of reflection/refraction laws (b) Schematics illustration of the operational principles of Filmetrics.	77
Figure 4.18:	Optical reflector meter, Filmetrics F-20.	77
Figure 4.19:	Image of UV-Vis-NIR Spectrometer system (Model: Cary 5000).	78
Figure 4.20:	The image of the Motic digital optical microscope (Model: BA310)	80
Figure 4.21:	Image of Solar Simulator system-IV (Model: KEITHLEY-2400 SOURCE METER).	81
Figure 4.22:	Schematic diagram of the fabrication process of PMMA/Si Fresnel lens starting from (a) RCA cleaning process, (b) spin coating of PMMA photoresist on the Si substrate, (c) development process of the exposed layer of PMMA and (d) Reactive ion etching process.	83
Figure 4.23:	Schematic diagram of the fabrication process of PMMA/SiO_2 Fresnel lens (a) Wafer cleaning process (b) Plasma exposure (c) Spin coating of PMMA photoresist on the Si substrate (d) Metal deposition (e) Electron beam lithography process (f) Reactive ion etching process (g) development process of the exposed layer of PMMA.	85
Figure 4.24:	Schematic illustration of the fabrication process of master mold (Si-Mold); (a) RCA cleaning process of Si substrate (b) Spin coating of PMMA photoresist on the Si substrate and baking (c) EBL process and Developing (d) Metal deposition (e) Lift off process (f) Reactive ion etching process.	88
Figure 4.25:	Schematic illustration of the fabrication process of PMMA/SiO_2 Fresnel lens using replica molding method	89

(a) PDMS mixture preparation and Poured on Si-Mold (b) Tearing of PDMS from Si-Mold (c) Clean the fused silica (SiO_2) (d) Spin coating of PMMA on SiO_2 (e) Imprint PDMS-Mold on PMMA/SiO_2 (f) Tear the PDMS from PMMA/SiO_2 to obtain PMMA/SiO_2 Fresnel lens.

Figure 5.1: FESEM image and the EDX spectrum of the crystalline Silicon substrate material after RCA cleaning steps; (a) EDX spectrum (b) FESEM image. 92

Figure 5.2: FESEM image and the EDX spectrum of the crystalline Silicon substrate-coated with PMMA resists; (a) EDX spectrum (b) FESEM image. 93

Figure 5.3: FESEM images of Fresnel rings on PMMA/Si surface (a) Array of Fresnel rings at 130X Magnification (b) Array of Fresnel rings at 500X Magnification (c) Fresnel rings at 4000X Magnification (d) Fresnel rings at 800X Magnification. 93

Figure 5.4: FESEM images showing the dimensions of Fresnel rings on PMMA/Si surface. 94

Figure 5.5: AFM analysis of surface morphology of crystalline silicon after RCA cleaning (a) 3-Dimensional topographic amage (b) 2-Dimensional view. 95

Figure 5.6: AFM analysis of surface morphology of crystalline silicon coated with PMMA film layer (a) 3-Dimensional topographic image (b) 2-Dimensional view 96

Figure 5.7: 2-Dimensional view of AFM images of the fabricated Fresnel rings at different magnifications: (a) $(20\ \mu m)^2$ (b) $(50\ \mu m)^2$ and (c) $(100\ \mu m)^2$ 96

Figure 5.8: 3-Dimensional view of AFM images of the fabricated Fresnel rings. 97

.

Figure 5.9: AFM images of Fresnel rings etched at 200 W RF-power and the process pressure of 20 mTorr, (a) 3-dimensional topology, (b) etching profile, (c) 2-dimensional view and (d) One complete unit of Fresnel rings at $(100\ \mu m)^2$ size. 98

Figure 5.10:	AFM images of Fresnel rings etched at 200 W RF-power and the process pressure of 15 mTorr, (a) 3-dimensional topology, (b) etching profile, (c) 2-dimensional view and (d) One complete unit of Fresnel rings at $(100\ \mu m)^2$ size.	99
Figure 5.11:	AFM images of Fresnel rings etched at 150 W RF-power and the process pressure of 15 mTorr, (a) 3-dimensional topology, (b) etching profile, (c) 2-dimensional view and (d) One complete unit of Fresnel rings at $(50\ um)^2$ size.	101
Figure 5.12:	AFM images of Fresnel rings etched at 150 W RF-power and the process pressure of 10 mTorr, (a) 3-dimensional topology, (b) etching profile, (c) 2-dimensional view and (d) One complete unit of Fresnel rings at $(50\ um)^2$ size.	102
Figure 5.13:	Depth profile of Fresnel rings on Si (a) AFM image showing EBL/RIE depth profile (b) A complete unit of Fresnel rings showing position of each radius (c) FESEM image of depth profile showing the width and the height of each ring.	103
Figure 5.14:	The FESEM image of 10 by 10 arrays Fresnel rings units on Si.	105
Figure 5.15:	UV-Vis-NIR reflection spectral analysis of three measured samples (a) Bare-Si (b) Si-coated with PMMA resist layer and (c) Si-Patterned with array of Fresnel rings.	108
Figure 5.16:	Reflection spectra comparing the light reflections of three measured samples.	108
Figure 5.17:	FTIR absorption spectral analysis on PMMA/Si with PMMA film layer of different thickness (a) Pure or uncoated Si (b) 150 nm PMMA film layer on Si (c) 301.6 nm PMMA film layer on Si (d) 316.1 nm PMMA film layer on Si.	111
Figure 5.18:	Comparisons between the FTIR absorption spectral on PMMA/Si with PMMA film layers of different thicknesses.	111
Figure 5. 19	FTIR reflection spectral analysis on PMMA/Si with PMMA film layer of different thickness (a) Pure or uncoated Si (b) 150 nm PMMA film layer on Si (c) 301.6	112

nm PMMA film layer on Si (d) 316.1 nm PMMA film layer on Si.

Figure 5.20: Comparisons between the FTIS reflection spectra on PMMA/Si with PMMA film layers of different thicknesses. 112

Figure 5.21: FESEM image and the EDX spectrum of the SiO_2 substrate material after cleaning steps (a) EDX spectrum (b) FESEM image. 115

Figure 5.22: FESEM image and the EDX spectrum of the SiO_2 after plasma exposure (A) EDX spectrum (B) FESEM image. 115

Figure 5.23: FESEM image and the EDX spectrum of the SiO_2 substrate-coated with PMMA resist (a) EDX spectrum (b) FESEM image. 116

Figure 5.24: FESEM image of the fabricated Fresnel lens on SiO_2 substrate. 116

Figure 5.25 Plot of Fresnel rings' radius against number of Fresnel zone Z, with graphical relationship of the errors occurred at each Fresnel zone. 118

Figure 5.26: The graphical relationship between the measured focal length of Fresnel lens and the wavelength of visible light. 118

Figure 5.27: Graphical relationship comparing the designed and measured focal lengths of Fresnel lens as a function of wavelength of visible light. 119

Figure 5.28: AFM images of the surface morphology of SiO_2 after DECON (a) 3-Dimensional topography (b) 2-Dimensional view. 120

Figure 5.29: AFM images of the surface morphology of SiO_2 after plasma etching (a) 3-Dimensional topography (b) 2-Dimensional view. 120

Figure 5.30: AFM images of the surface morphology of SiO_2-coated with PMMA film layer (a) 3-Dimensional topography (b) 2-Dimenssional view. 121

Figure 5.31:	AFM images of the fabricated Fresnel lens on SiO_2 (A) 2-Dimenssional topography (b) 3-Dimensional view and (c) Lens' facet profile.	121
Figure 5.32:	Optical Microscope image of Fresnel lenses array captured by the image sensor for the intensity distribution on the focal plane of each lens.	122
Figure 5.33:	Optical Microscope image of Fresnel lens at high magnification.	123
Figure 5.34:	The images of Fresnel lens captured by the image sensor for the intensity distribution on the focal plane.	123
Figure 5.35:	Graphical representation of the intensity distribution on the focal plane.	123
Figure 5.36:	Comparison between the FTIR transmission spectral analyses of different thickness of PMMA film layer on SiO_2.	127
Figure 5.37:	FTIR absorption spectral analysis (a) Infrared absorption on an uncoated SiO_2 (b) Infrared absorption on PMMA/SiO_2 with 250 nm thickness of PMMA (c) Infrared absorption on PMMA/SiO_2 with 274.4 nm thickness of PMMA (d) Infrared absorption on PMMA/SiO_2 with 480.8 nm thickness of PMMA.	128
Figure 5.38:	Comparisons of the FTIR absorption spectral analysis of the PMMA/SiO_2 with PMMA layer of different thicknesses.	128
Figure 5.39:	UV-Vis-NIR Transmission spectral analysis of three measured samples (a) Transmission through PMMA/SiO2 with 250 nm thickness of PMMA (b) Transmission through PMMA/SiO2 with 274.4 nm thickness of PMMA, and (c) Transmission through PMMA/SiO2 with 480.8 nm thickness of PMMA	130
Figure 5.40:	UV-Vis-NIR Transmission spectra comparing the light transmission at three different thicknesses of PMMA.	131
Figure 5.41:	FESEM images pattern of Fresnel rings on Ni/Si at different magnifications and the EDX spectrum (a) 2-Dimensional image at 140X, (b) 2-Dimensional image at	134

500X, (c) 2-Dimensional image at 1KX, (d) EDX spectrum and (e) 3-Dimensional image at 10KX.

Figure 5.42: FESEM images pattern of Fresnel rings on Si at different magnifications after etching (a) 2-Dimensional image at 1KX, (b) 2-Dimensional image at 30KX, and (c) 2-Dimensional image at 30KX showing the dimension of ring thickness. 134

Figure 5.43: AFM images of Fresnel rings array on Si etched with SF_6/O_2 etchant (a) 3-Dimensional view (b) Etching profiles and (c) 3-Dimensional view. 136

Figure 5.44: AFM images of Fresnel rings array on Si etched with SF_6 etchant (a) 3-Dimensional view (b) Etching profiles and (c) 3-Dimenssional view. 136

Figure 5.45: Experimental set-up of micro array of Fresnel lenses CPV-system on Si solar cells. 140

Figure 5.46: IV-characteristics of Si-Solar cells comparing the results of the three experimental stages for Si-Solar Cells only, Si-Solar Cells with PMMA/SiO_2 placed at $20\ \mu m$ and Si-Solar Cells with PMMA/SiO_2 Fresnel lenses array placed at $45\ \mu m$. 142

LIST OF ABBREVIATIONS

eV	Electron-volts
PV	Photovoltaic
CPV	Concentrator Photovoltaic
EBL	Electron beam lithography
Si	Silicon
SiO_2	Silicon dioxide/Fused Silica
PMMA	Poly (methyl methacrylate)
PDMS	Polydimethylsiloxane
MEMS	micro-electro-mechanical system
Si	Silicon
nm	Nanometer
USM	Universiti Sains Malaysia
NOR	Nano-Optoelectronics Research and Technology
RIE	Reactive ion etching
RF	Radio Frequency
EJCRP	Europe-Japan Collaborative Research Project
PC	Polycarbonate
PVC	Polyvinyl chloride
AC	Alternating Current
DC	Direct Current
SEM	Scanning Electron Microscope
WD	Working Distance
SPL	Single Pass Line
μC	Micro-Coulomb
μm	Micro-Meter
nm	Nano-Meter
SE	Secondary Electron
RCA	Radio Corporation of America
DECON	Decontaminations

rpm	Revolution Per Minute
GDSII	Graphic Database System II
MIBK	Methyl isobutyl ketone
IPA	Iso-propyl alcohol
DI	De-ionized
Ni	Nickel
ICP	Inductive Couple Plasma
PE	Plasma Etching
PECVD	Plasma-Enhanced Chemical Vapor Deposition
MHz	Mega Hertz
SCCM	Cubic Centimeters Per Minute
STP	Standard Temperature and Pressure
FESEM	Field Emission Scanning Electron Microscope
EDS/EDX	Energy Dispersive X-Ray Spectroscopy
STEM	Scanning Transmission Electron Microscope
EBSD	Electron Backscatter Diffraction
AFM	Atomic Force Microscope
FTIR	Fourier Transform Infrared Spectroscopy
IDDQ	Integrated Circuit Quiescent Current
HMDS	Hexamethyldisilazane
CHF_3	Trifluoromethane
LED	Light Emitting Diode
ARC	Anti-Reflection Coating

LIST OF SYMBOLS

V_{Max}	Maximum voltage
V_{OC}	Open Circuit Voltage
I_{Max}	Maximum Current
I_{SC}	Short Circuit Current
J_{SC}	Short Circuit Current Density
R_s	Series Resistance
R_{sh}	Shunt Resistance
P_{Max}	Maximum Power
FF	Fill factor
W	Watts
s	Seconds
K	Kelvin
^{O}C	Degree Celsius
I-V	Current and Voltage
I_O	Saturation current of the diode
I_{ph}	Light generated current
K_B	Boltzmann constant
T	Temperature/Gratings Period
P_{in}	Power due to incident light
ɳ	Efficiency
Q	Electric charge
Q_E	Quantum Efficiency
Q_{EE}	External Quantum Efficiency
Q_{EI}	Internal Quantum Efficiency
$\boldsymbol{\lambda}$	Wavelength
$\boldsymbol{\phi}$	Solar flux
S ($\boldsymbol{\lambda}$)	Spectral Response
h	Plank's Constant/Fresnel lens Height

J	Joules
E_λ	Radiant energy per unit volume
λ_{Max}	Maximum Wavelength
ε	Emission spectra/Emissivity
k	Extinction Constant/Wave Number
σ	Stefan-Boltzmanns' constant
UV	Ultraviolet Light
VIS	Visible Light
IR	Infra-red Light
Z^O	Solar zenith angle
AM	Air Mass
I_{Tatal}	Total Solar Radiation Intensity
I_{Direct}	Direct Solar Radiation Intensity
$I_{Diffused}$	Diffused Solar Radiation Intensity
$\vec{E}$	Electric Field Intensity
$\vec{B}$	Magnetic Field Intensity
θ_i	Angle of Incidence
θ_r	Angle of Reflection
θ_t	Angle of Refraction
n	Refractive Index
τ	Transmission Coefficient
α	Absorption Coefficient
ρ	Reflection Coefficient
ω	Rotational Speed
V	Accelerating Voltage
I_B	Beam Current
A_{SS}	Area Step Size
A_{DT}	Area Dwell time
A_{Dose}	Area Dose
A_{BS}	Area Beam Speed

L_{SS}	Line Step Size
L_{DT}	Line Dwell time
L_{Dose}	Line Dose
L_{BS}	Line Beam Speed
f	Focal Length
f_{number}	Relative Aperture
f_D	Designed Focal Length
f_M	Measured Focal Length
z	Number of Fresnel Ring/Fresnel Zone
R	Radius of Fresnel Rings
D	Diameter of Fresnel Rings
J_1	First Order Bessel Function
δ	Duty Ratio
$\varphi_{(x)}$	Phase-Retardation Function of the Gratings
m	Order of Diffraction waves
R_q	Root Means Square Surface Roughness
d	Depth of Fresnel Rings
R_{int}	Internal Radius of Fresnel Rings
R_{ext}	External Radius of Fresnel Rings
$A_{F-rings\ unit}$	Increase in Area of Fresnel Rings Unit
$A_{}$	Increase in Area due to Formation 100-Units of Fresnel Rings
A_{eff}	Effective Area
Ω	Ohms

APLIKASI MIKRO KANTA FRESNEL DALAM PENINGKATAN OUTPUT SEL SURIA

ABSTRAK

Kanta Fresnel sudah lama digunakan dalam aplikasi fotovolta penumpu untuk menumpukan sinar tuju suria ke atas sel-sel suria, namun, sistem ini terjejas disebabkan jarak fokusnya yang panjang, pencahayaan di atas sel suria yang tidak seragam dan ia memenuhi kawasan yang lebih luas bagi sel-sel suria. Tesis ini memberi tumpuan kepada penggunaan tatasusunan kanta Fresnel Poly (methyl methacrylate) (PMMA) dengan saiz yang lebih kecil dan jarak fokus yang lebih pendek (dalam ukuran mikrometer) sebagai penumpu sistem fotovolta (CPV) di atas sel suria silikon. Sistem ini telah difabrikasi menggunakan kombinasi teknik litografi alur elektron (EBL) proses punaran ion reaktif (RIE) dan teknik membentuk replika Polydimethylsiloxane (PDMS). Hasil kajian menunjukkan bahawa, system CPV yang mempunyai kanta Fresnel dengan diameter luaran maksimum $45.24\ \mu m$, memberikan 3025-tenaga suria per cm^2 dengan panjang fokus f dianggarkan bernilai $45\ \mu m$. Kecekapan penghantaran sebanyak 93.7 % telah dicapai pada sudut tuju $\approx 0^o$ dengan nombor $f \leq 1$ dan nisbah penumpuan optic (OCR) sebanyak 95X. Apabila sistem tatasusunan kanta Fresnel yang terhasil diletakkan pada titik fokus ($\approx 45\ \mu m$) dari permukaan sel suria silicon (Sel suria-Si) didapati ia meningkatkan voltan litar terbuka V_{OC} dari 538.83 mV kepada 556.73 mV, ketumpatan arus pendek J_{SC} dari 11.46 mA/cm^2 kepada 16.66 mA/cm^2 dan kuasa maksimum P_{max} dari 21.64 mW ke 33.06 mW. Sementara itu, sistem ini juga meningkatkan kecekapan penukaran kuasa Sel suria-Si dari 9.01 % ke 9.18 % dan menurunkan rintangan bersiri

R_s bagi sel suria-Si tersebut daripada 1.95 Ohms kepada 1.14 Ohms. Secara umumnya, keputusan-keputusan ini jelas menunjukkan kelebihan menggunakan sistem CPV bersaiz kecil dalam menyiasat peningkatan parameter-parameter cirian output sel suria silikon. Oleh itu, sistem ini pastinya mempunyai potensi yang besar dalam sel-sel suria yang menggunakan bahan-bahan lain.

APPLICATION OF MICRO FRESNEL LENSES IN OUTPUT ENHANCEMENT OF SOLAR CELLS

ABSTRACT

Fresnel lens have been used in concentration photovoltaic applications to converge the incident solar irradiance on to the solar cells. However, this system suffers from long focal distance, non-uniform illumination on the solar cells and it occupies larger area as compared to that of solar cells. This thesis focuses on the use of smaller size with shorter focal distance (in micrometers) Poly (methyl methacrylate) (PMMA) Fresnel lenses array as a concentrator photovoltaic (CPV) system on silicon solar cells. The system was fabricated using the combinations of the electron beam lithography (EBL) the reactive ion etching (RIE) and the Polydimethylsiloxane (PDMS) replica molding techniques. The results obtained shows that, CPV system containing Fresnel lenses with maximum external diameter of $45.24\ \mu m$, have 3025-suns per cm^2 with the approximate focal length f of $45\ \mu m$. The transmission efficiency of 93.7 % was achieved at an angle of incidence of $\approx 0^o$ with $\mathrm{f-number} \leq 1$ and the optical concentration ratio (OCR) of 95X. The resulting Fresnel lenses array system when place at the focal point ($\approx 45\ \mu m$) from the surface of silicon solar cells (Si-Solar cells) increased the open circuit voltage V_{OC} from 538.83 mV to 556.73 mV, short current density J_{SC} from 11.46 mA/cm^2 to 16.66 mA/cm^2 and the maximum power P_{max} from 21.64 mW to 33.06 mW. Meanwhile, this system also enhanced power conversion efficiency of Si-Solar cells from 9.01 % to 9.18 % and decreased the series resistance R_s of Si-Solar cells from 1.95 Ohms to 1.14 Ohms. In general, these results clearly indicate

the advantage of using small size CPV-system in investigating the improvement in the output characteristic parameters of silicon solar cells. Thus, conclusively, the system has the great potentiality in other material solar cells.

CHAPTER 1

INTRODUCTION

1.1 Overview

Crystalline silicon solar cells is the most appropriate type of energy generation devices for both space and terrestrial applications, which have been used to power satellites and shuttles as well as small and large scale power generation in the terrestrial applications. As the energy consumption rate in the world is increasing every year, where most of the energy sources come from fossil fuels and nuclear power generations, which are high material cost, requires high cost of maintenances, and polluting the environment. With these disadvantages associated with the above energy sources and the exhausted nature of the sources, it is necessary to incorporate the use of renewable energy sources such as solar and wind.

Crystalline silicon PV solar cells have been developed to harness the Sun's light energy in to electricity, and the fundamental problem associated with solar cells is the low-efficiency. To address this problem; many researches are continuing all over the world in to ways and means of enhancing the performance efficiency of solar cells. Among such means are the use of thinner wafer, thin film solar cell technologies and optical concentration technologies (K.-K. Chong et al., 2013). Optical concentration technique is one of the simplest and cheapest methods used today for the improvement of the performance efficiency of solar modules/panels.

The most common solar cells used today are made up of crystalline silicon materials which can either be single crystalline or polycrystalline. Although the mean-full efficiency was achieved with single crystalline silicon solar cells, the silicon solar cells have high cost of purchase. This is because, silicon is an indirect

band gap semiconductor that requires a thick absorber layer (of about 250-400 μm thick) to absorb higher percentage of the sunlight for the conversion in to electricity (Ibrahim and Kamarulazizi, 2003).

In recent years, many efforts have been devoted in developing low-cost and high efficient solar cells for the use in both space and terrestrial energy generation (K. Chong et al., 2013). Producing low-cost, high efficient solar cells can be achieved by optical concentration technology; by using appropriate material to fabricate Fresnel lens with high concentration ratio on a single crystalline silicon solar cell, which can transmit more solar radiations on to the solar cell.

Optically concentrated PV solar cells (in Fresnel configurations) provide the best hope to obtain high efficient and low-cost solar cells (Khamooshi et al., 2014). Two compounds, Silicon dioxide, and Poly (methyl methacrylate) are the most promising materials for achieving these goals because they have exceptional characteristics particularly for single crystalline silicon solar cells.

1.2 Motivations and problems statement

Having satisfied with the fact that, PV is the most promising field among various renewable energies, it is equally important to make solar cells durable, reliable, available, profitable as well as affordable to the market. Therefore the focus should not be restricted only on enhancing the performance efficiency and the stability of the solar cells, but also trying to find the techniques of improving the rate of production at low cost without degrading the quality.

The fabrication processes and the cost of materials (e. g. glass) for producing the optical lenses and mirrors used for the concentrator photovoltaic (CPV) systems at the present day lead to the solar modules are available at high-cost per unit.

Modern computer-controlled fabrication methods like electron beam lithography (EBL) and photolithography using low-cost and available materials (e. g. silica (SiO_2) as a substrate and PMMA as photo resist) offers a high possibility of producing higher optical quality Fresnel lens than the finest glass one. In addition, these methods are widely used for the designing of most of the electronic components (e. g. Integrated circuit IC, Transistors) (Mohammad Ali Mohammad et al., 2012). The major advantages of PMMA are; low absorption band (of wave number between 2000 cm^{-1} and 2750 cm^{-1}), availability and wider applications in engineering, medical as well as daily-life purposes (Tsui et al., 2012). In addition to these, PMMA is a lightweight material with shatter-resistance used in the micro-electro-mechanical system (MEMS) process as a photoresist to provide high-contrast and high-resolution images. The optical properties of PMMA show that it can be used for mid-infrared lenses. On the other hand, silicon has very high transmission efficiency from 2 to 6 μm with the band gap of 1.14 eV at room temperature (25 ^oC) and 1.17 eV at temperature of 0 K. It is a non-toxic and light weight material with very good strength, and is thermally stable. It is also inert to most chemicals, and is readily available and it is low cost (Tamarack St. and Bozeman, 2011). The optical and the electrical properties of silicon can be controlled by adding dopant to the pure silicon; the transmission and resistivity decreases with the increase in doping. But the presence of oxygen has a minimal impact on the transmission for mid-wave infrared applications. Finally, having regards to the mentioned properties of SiO_2 and PMMA, and the advantages of using soft lithography methods for the fabrication of Fresnel lens in CPV systems. Although, PMMA Fresnel lenses array CPV-system fabricated by soft lithography technique requires both physical and engineering knowledge to develop the system for the first time thereby making it costly compared

to conventional methods. But the subsequent productions can be achieved using either or both the Si-Mold and/or the PDMS-Mold of the system structures by simply be copying and imprinting the structures onto several supporting frame producing as many as possible CPV-systems. Thus, the possibility of producing high quality product of CPV solar cells with low-cost, available and affordable with low energy pay-back time is promising. However, silicon can be used for lenses, but it is fragile and hardness may lead to the fabrication process be complicated and time consuming. However, the light transmissions of polymer materials like PMMA is seriously affected by its thickness (Tsui et al., 2012).

Unlike conducting and semiconducting substrates, polymers resist layers on insulators accumulate more charge during EBL exposure process which deflects the e-beam and distorts the pattern, but this can be addressed by the use of conducting anti-charging layers like thin film (5 nm-thick) of either Al, Cr, or Cu. However, such a coating layer results in e-beam scattering in metal layer and subsequent broadening the exposure profile in the resist which limit the resolution at the deep nano-scale and also tends to decrease sensitivity of the process (Mohammad Ali Mohammad et al., 2012).

1.3 Objectives of the Research

The general objective of this research work is to use micro-scale array of Fresnel lenses as a concentrator photovoltaic system on the surface of silicon solar cells and the sub-objectives are as follows;

1. To fabricate Fresnel lens by soft lithography method.
2. To study the optical properties of PMMA resist on a Si and SiO_2 substrates.

3. To form an array of Fresnel lenses as a photovoltaic concentrator.
4. To study the improvement in the power output from the solar cells by the use of the array.

1.4 Research originality

The novel contributions of this research work are as follows;

1. Fabrication of Si Fresnel rings of vertical sidewalls profile.
2. Fabrication of smooth Si surface on the location between Fresnel rings.
3. Fabrication of SiO_2 Fresnel lens by electron beam lithography EBL.
4. Fabrication of PMMA Fresnel lenses array by the combinations of the EBL, the RIE and the PDMS replica molding techniques.
5. The used of small scale (micro-scale) Fresnel lenses array as a PV concentrator system on silicon solar cells.

1.5 Scope of thesis

This work limited to the investigation of the fabrication process of micro Fresnel lenses for CPV application. Even though a number of studies have been carried out and demonstrated on the uses of micro-lenses for CPV-system devices, limited information is available in understanding the soft lithography process and linking the process in CPV-systems device application. This study is an attempt to fill in the gap in understanding the underlying physics behind the micro fabrication process especially the plasma etching interaction with materials and micro optics. This work also demonstrates the applications of micro Fresnel lenses for output enhancement from crystalline silicon solar cells.

1.6 Thesis Outline

The outlines of this thesis can be summarized as follows: Chapter 1 presents the introduction on the important applications of crystalline silicon solar cells, while chapter 2 discusses the literature review on the use of Fresnel lens for concentrated photovoltaic application. The general principles and theories of Fresnel lenses in CPV applications as well as the principles of micro/nano-fabrication methods are discussed in Chapter 3. The details description on the methodology adopt in this work and number of micro/nano-fabrication equipment in the USM NOR lab facilities utilized in this research work, as well as the materials characterizations used in the research work are discussed in chapter 4. Chapter 5 describes the experimental results for fabrication and characterization of micro array of Fresnel rings on Si by EBL and RIE processes, the experimental results for the fabrication and characterization of Fresnel lens on PMMA/SiO_2 by EBL and RIE processes, as well as the experimental results for the fabrication and characterization of micro array of PMMA Fresnel lenses by replica molding method. This chapter also presents the results on improvements in the characteristic parameters of solar cells by solar simulator (IV). Finally, chapter 6 presents the conclusions and recommendation for future works.

CHAPTER 2

LITERATURE REVIEW

2.1 Introduction

This chapter reviews the available and related literatures. It discusses the available literatures on solar photovoltaic concentrator systems. The literatures on Fresnel lenses as CPV systems and the literatures on the use of micro-optics in CPV systems applications are also discussed in this chapter.

2.2 Concentrator PV systems

Since the amount of electric current generated from solar cells/panel is proportional to the amount of the incident solar radiation on the solar cells. Optical lenses and reflectors can be employed to maximise the amount of the sunlight striking onto the surface of the cells. Recently, the results of the Europe-Japan Collaborative Research Project (EJCRP) on photovoltaic concentrators shows that, the world record of the energy efficiency under $240\ to\ 305$ suns in InGaP/GaAs/InGaAs triple junction solar cell was found to be up to 43.5% (Yamaguchi and Luque, 2013).

Paul and his co-workers had compared the experimental characteristics of an isolated PV module with and without compound parabolic concentrator using mobile solar simulator. The acceptance half-angle of compound parabolic concentrator is 30^{o} and the truncated geometrical ratio is 1.96. They observed that, there are variations in the amount of the energy flux concentration on the surface of the module; large amount of energy flux were concentrated at the edges of the receiver. Although the output power of the module with the compound parabolic concentrator

is greater than without, the compound parabolic concentrator having the problems of non-uniform illumination on the receiver (Paul et al., 2013).

Sangani and Solanki, had developed V-trough concentrator (2-sun) system with the geometric concentration ratio of 2 (2-sun) using tracking models. They evaluated the photovoltaic modules under 2-sun concentrator and observed that the output power of the PV module increases by 44% when compared to the PV flat-plate system for passively cooled modules (Sangani and Solanki, 2007).

In a related development, Chong and his team (Chong et al., 2013), revised several literatures in their paper titled "design and development in optics of concentrator PV systems". In their paper, they presented detailed architectural design and optical principle of solar concentrators of various research works for the past 30 years done by many researchers, which includes the work lead by Leutz and his team (Leutz et al., 1999) where they designed an optimum convex shaped non-imaging Fresnel lens according to the edge ray principle in which, the radiant energy will be well distributed over the photovoltaic panel if a secondary concentrator and a diffuser are provided. Another work revised by Chong and his team is that of Jebens and Skillman in which they patented Fresnel lens concentrator formed by a specially designed Fresnel lens and a solar cell located on the axis of the lens at its focal plane. The design of the lens is made in such a way that the central facets of the lens will progressively be projecting the solar radiations towards the outer periphery of the solar cell and the facets will progressively be projecting the radiation toward the centre of the solar cell on one hand and adjacent groups of facets of the lens projects the radiation alternatively in front and beyond the solar cell. The first was to obtain a uniform distribution of light on the solar cell while the second was to maintain a constant light intensity for a certain depth of focus of the lens. Finally, they

concluded that optical concentration PV system is the best way of producing high efficient, low cost, harmless to the environmental conditions, easy to maintain and simple to manufacture (K.-K. Chong et al., 2013).

Whitfield and his co-workers compares Point focus Fresnel lens, two-axis tracking, and the use of the housing as heat sink with other models which comprises a linear Fresnel lens, solid compound parabolic collector CPC, secondary's, and the two-axis tracking. The linear Fresnel lens system has the advantage of being simple and totally enclosed yet is more costly than some of the others. Conversely, the point-focus Fresnel lens has the advantage of having potential for simple mass-produced optics but its serious problem is the loss of efficiency at higher concentration (Whitfield et al., 1999).

Khalifa and Al-Mutawalli conducted an experimental study on effects of two-axis sun tracking on thermal performance of compound parabolic collector CPC in two different modes; in the first, a batch feeding was used where no flow through the collector was allowed whereas in the second, different steady water flow rates were used. Based on the results obtained, they concluded that the energy gain of a CPC collector can be increased by using two-axis tracking systems. The best improvement was achieved when the flow rate was in the range of 25 to 45 kg/hr (Khalifa & Al-Mutawalli, 1998).

Mallick and his team, designed a novel non-imaging asymmetric compound parabolic photovoltaic concentrator (ACPPVC) with different numbers of photovoltaic PV, strings connected in series. Experimentally characterization of the system was conducted under outdoor conditions both with and without concentrators which indicated that the use of an ACPPVC increased the maximum power point by 62% when compared to a similar non-concentrating PV panel (Mallick et al., 2004).

2.3 Fresnel lens CPV system

Fresnel lenses find very wide applications in modern actively developing PV systems and becoming the backbone of the solar concentrators in different photovoltaic solar cells and panels (Shvarts and Soluyanov, 2011). This is because most of the Fresnel lenses are plano-convex, thin, and aspheric with low f-number, thus they have very strong asymmetric behaviour, and therefore, they are applicable in almost all sectors of optical technology, hence, they play a vital role in CPV systems. Developments of Fresnel lens for photovoltaic concentrators have been studied. In the recent years, several methods of photovoltaic concentrators with Fresnel lens using different materials have been investigated.

Ryu and co-workers proposed a new configuration of CPV system utilizing modularly faceted Fresnel lenses to achieve a uniform intensity on the solar cells with moderate concentration ratio. Fig. 2.1 reveals that the uniform illumination is obtained by the superposition of flux distribution resulted from modularly faceted Fresnel lenses. The flux distributions at the solar cell plane are estimated to be uniform within $\approx 20\%$ with transmission efficiency greater than 65% for 3×3, 5×5 and 7×7 arrays of Fresnel lenses. With $f/1.2$, the intensity levels of various concentration ratios are $7 - suns$ for the 3×3 array, $19 - suns$ for the 5×5 array, $31 - suns$ for the 7×7 array, $47 - suns$ for the 9×9 array, and $60 - suns$ for the 11×11 array, respectively (Ryu et al., 2006).

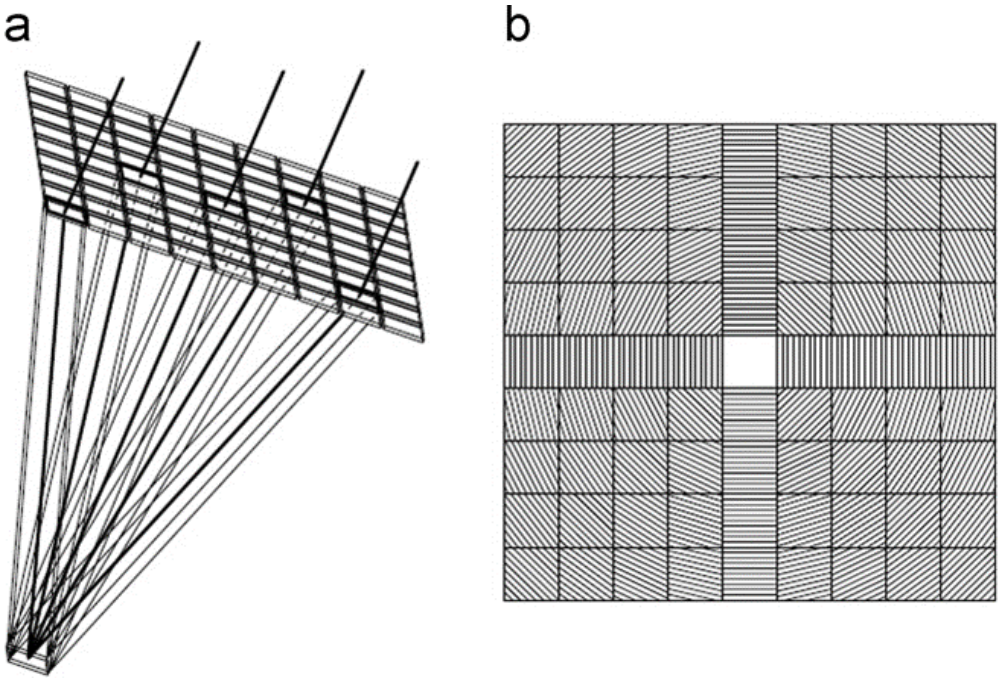

Fig. 2.1: Optical design concept of modular Fresnel lenses for solar flux concentration (a) 3-D of concentration optics (b) facet directions of modularly faceted Fresnel lenses (Ryu et al., 2006).

Chen and Su, presented the simulation results on Fresnel lens and secondary optical elements as a CPV system by the ray tracing method using advanced system analysis program (ASAP) software, in which the comparison between the estimated optical efficiencies and the acceptance angles of a Fresnel lens concentrator (i.e. without secondary optical element (SOE), a Fresnel lens concentrator with Reflective Pyramid as a SOE, a Fresnel lens concentrator with a Reflective Cone Type as a SOE, and a Fresnel lens concentrator with a Refractive Dome Type as a SOE are made respectively). The simulation results show that the concentrator containing the reflective cone type as a SOE have the highest optical efficiency compared to the rest. Hence, they studied the optimization of the concentrator with cone type as a SOE and found the improvement in acceptance angle and uniformity of the solar radiation on the surface of the solar cells (Y. Chen and Su, 2010).

Miñano and co-workers designed and fabricated a multifunctional concentrator PV system called Fresnel Kohler (FK-concentrator) by Kohler integration principles, in which a PMMA Fresnel lens with four identical quadrants (as a primary optical element (POE)) along with a free-form of glass-molded lens with four identical sectors (as a secondary optical element (SOE)) are arranged in form of Kohler array. Thus each pair of a quadrant and a sector works together as a Kohler integrator couple. The electrical efficiency of 32.7% and fill-factor of 84.6% on triple junction solar cell at the operating temperature of 25^oC was achieved with this FK-concentrator having 710X concentration ratios and $\pm 1.27^o$ as a concentrator's acceptance angle (Miñano et al., 2013).

On the other hand, Languy and his team, demonstrated the feasibility of obtaining a Fresnel lens with high concentration ratio operating with wavelengths between 380 nm and 1600 nm via PMMA and Polycarbonate PC in which the linear chromatic aberration of a singlet and doublets hybrid lenses were compared. Their result shows that for singlet lenses at normal incidence, the maximum theoretical concentration ratio of 1000X can be obtained, while for hybrid lenses, the concentration ratio increases to 5000X and that of refractive doublets is about 2×10^6. They also achieved in maximizing the radiation flux density on the solar cells by determining the ideal focal point as a function of linear chromatic aberration and the geometric concentration (Languy et al., 2011).

Another research lead by Kusko, simulated a Fresnel lens and binary phase gratings via glass of refractive index $n = 1.5$ by Beam Propagation Method, compared the results obtained with the theoretical and finds out that the results were closed to the theoretical values. Therefore, Beam Propagation Method can be used to simulate other complex optical devices (Kusko et al., 2009).

In a related development, Jing and co-workers studied the optical performance of the compound Fresnel lens as a concentrator photovoltaic system comprising saw teeth Fresnel lens as a primary optical element and ring type Fresnel lens as secondary optical element. In-line with this, the improvements in the acceptance angle, the uniformity in the solar radiation on the solar cell, and reduction in the aspect ratio were significantly studied in which higher optical efficiency and smaller aspect ratio were achieved (Jing et al., 2011).

Arnaoutakis and his team, studied the enhancement in conversion efficiency of a planar bifacial silicon solar cell (SC) together with a 25% Er3þ doped hexagonal sodium yttrium fluoride (β-NaYF4:Er) up-concentrator (UC) phosphor by the integration of compound parabolic concentrating optics (CPCs). In their study, they achieved in obtaining an efficiency increase of 32% and an enhancement in external quantum efficiency (EQE) from 1.33% for the non-concentrating reference UC-SC to 1.80% for a solar cell with integrated optics for an excitation at 1523 nm with an irradiance of 0.024 W/cm^2, corresponding to a normalized EQE of 0.75 W/cm^2. Thus they conclude that their results demonstrates that CPCs are suitable for UC-SC as they increase the concentration in the forwards direction, while maintaining high collection efficiency of the UC emission in the reverse direction (Arnaoutakis et al., 2015).

Solano and co-workers developed a model for theoretical investigation of the effect of inserting a buffer layer between a periodically multi-layered isotropic dielectric (PMLID) material acting as a planar optical concentrator and a photovoltaic solar cell considering the crystalline silicon (c-Si) and gallium arsenide (GaAs). Their results shows that, the buffer layer can act as an antireflection coating (ARC) at the interface of the PMLID and the photovoltaic materials, and its structure

can increase the spectrally average electron-hole pair density by 36% for crystalline silicon solar cells c-Si, and 38% for gallium arsenide (GaAs) when compared to the structure without buffer layer. However, numerical evidences indicate that the optimal structure is robust with respect to small changes in the grating profile of the buffer layer (Solano et al., 2015).

Kocher-Oberlehner and his team, developed a planar photonic solar concentrator (PPC) by Langmuir–Blodgett (LB) technique onto clear 3 mm-thick polymethylacrylate (PMMA) sheets of 24 cm by 24 cm size with a silicon solar cell attached to the edge. The resulting periodic colloidal photonic crystals (PhCs) layer scattered the incident light into a waveguide mode and guided via total internal reflection to the edge mounted silicon solar cell. Depending on the size of the beads forming the photonic crystal film, the transmission and the reflection measurements taken in different geometries indicates rapid increased scattering of the incident light over a wide range of wavelengths. The I-V measurements on silicon solar cells attached to one side of a sheet with 8 layers of 250 nm beads exhibit a relative increase in efficiency by a factor of up to 3 as compared to the blank PMMA sheet. Thus, they concluded that these planer concentrators can increase the power output from photovoltaic cells without the need for solar tracking and have the potential of achieving a lifetime matching standard silicon solar cells (Kocher-Oberlehner et al., 2012).

Sun and co-workers, proposed a narrow rectangular channel receiver for direct liquid-immersion of silicon solar cells in linear concentrator photovoltaic (CPV) systems using dimethyl silicon oil with viscosity of $2\,mm^2/s$ as an immersion liquid by computational fluid dynamics (CFD) simulation and carried out the experimental investigations of the effects of liquid thickness on silicon solar cell

efficiency. Experimental results shows that silicon solar cell efficiency decreases with increasing thickness of immersion liquid, and hence, they noted that silicon oil thickness on top of the cell should be lower than 12 mm in order to achieve a cell efficiency promotion by liquid immersion. However, the CFD simulation results show that smaller channel makes for better heat transfer performance but larger flow resistance, and therefore their recommendations on the optimal channel height is that, it could not exceed 10 mm height. Furthermore, according to the force analysis result, they recommended that cover glass thickness should not be less than 3 mm and the width should be within 85 mm. Based on their predicted results of the optimized receiver, the silicon solar cells working under medium concentration (10–100X) can be controlled between the temperatures of 302 K and 340 K with Reynolds number (R_e) range of 7500–15,000 at the inlet temperature of 298.15 K. (Y. Sun et al., 2016).

El Daif and his team investigated the effects of silver nano-discs made by hole-mask colloidal lithography on the spectrally resolved efficiency of thin film crystalline silicon solar cells. The integration of Plasmon allows increasing the absorption of the structure and hence increases the internal quantum efficiency of crystalline silicon solar cells and it shows some improvement when compared to silicon solar cells without the silver nano-discs. The results on the reflection measurements shows that, the reflections increases as the thickness of nano-discs increases and slightly sloping down with the increase in wavelength of light, in which the reflection of 25% was observed at the wavelength of 600 nm for nano-disc of 50 nm-thick and 15% for nano-disc of 30 nm-thick. The internal quantum efficiency (IQE) on the other hand, decreases with the increase in nano-discs diameter. Over 80% IQE was obtained equivalent to the nano-disc diameter of 40 nm

at the wavelength of 600 nm and less than 80% IQE was obtained equivalent to the nano-disc diameter of 60 nm. Thus they recommended that Plasmonic particles should be integrated on the back of silicon cells, which will allow acting on light which would mostly be lost otherwise, and benefiting from Fano interferences which would act positively in the applications silicon solar cells (El Daif et al., 2012).

Sark developed a modelling for the current status of luminescent solar concentrators (LSCs) for mono-crystalline silicon mc-Si, gallium arsenide (GaAs), and InGaP solar cells by designing and comparing with experimental results. The modelling result on the concentrator shows that the LSC consists of a PMMA plate (refractive index $n = 1.49$, absorption $1.5\ m^{-1}$) doped with two luminescent dyes, CRS040 from Radiant Color and Lumogen F Red 305 from BASF with internal quantum efficiency (IQE) of 95%. The conversion efficiency of this LSC was modelled to be 2.45%. However, in comparison with the reviewed experimental results, Sark, found out that the GaAs, has the highest external quantum efficiency EQE, than mc-Si, within the wavelength ranges between 400 nm and 600 nm (van Sark, 2013).

Chen and co-workers fabricated biometric nanostructures of PMMA layer by the combinations of colloidal lithography, cast molding method, and reversal nano-imprint lithography techniques. The resulting biomimetic nanostructures reduce the average reflectance from 13.2% to 7.8% and enhanced power conversion efficiency of mono-crystalline silicon solar cells from 12.85% to 14.2%. Therefore, they recommended that, the biometric nanostructures of PMMA layer have a broadband antireflection coating AR, response and wide incident angle range, hence, they have the potential to replace conventional single-layer AR coatings for optical and electro-optical device applications (J. Chen et al., 2011).

This work is devoted to micro-fabrication of Fresnel lenses by soft lithography techniques for CPV application. However, limited literature reported on the use of this method for CPV application in silicon solar cells. Unlike other conventional photovoltaic concentrators in which the concentrator systems have large surface area as compared to that of solar cells, hence, are placed far away from the surface of the solar cells, this system have the same size as solar cells and hence, is placed on the surface of the solar cells without occupying any additional surface area in the space.

CHAPTER 3

PRINCIPLES OF FRESNEL LENSES CPV-SYSTEM, SOLAR CELLS AND MICRO/NANO-FABRICATION IN OPTICAL APPLICATIONS

3.1 Introduction

This chapter describes about the principles of Fresnel lenses CPV-system, materials and the operational principles of semiconductor devices. The chapter deals with P-N Junction, and the principles of Solar cells. The chapter will also consider the crystalline silicon solar cells and give detail explanations on the concept of optics and the used of optical lenses as concentrator photovoltaic system. Finally, the chapter will also give detail description of micro/nano-fabrication techniques and their applications in concentration photovoltaic systems.

3.2 Principles of Fresnel lenses CPV-system

The spectral response of crystalline silicon solar cells is critically dependent on the number of incident photons absorbed especially from far infrared to the red-end region of visible light. To achieve high magnitude light trapping system which can improve the internal quantum efficiency of crystalline silicon solar cells, micro array of Fresnel lenses could be a better solution. Micro array of Fresnel lenses CPV-system can suppress surface reflection, enhancing the absorption of light and could replace conventional CPV-systems in crystalline silicon solar cells applications. In this work, we fabricated micro-array Fresnel lenses CPV-system on Silicon solar cell. Fig. 3.1 shows the schematics illustration of PMMA/SiO_2 Fresnel lenses array on Silicon solar cells.

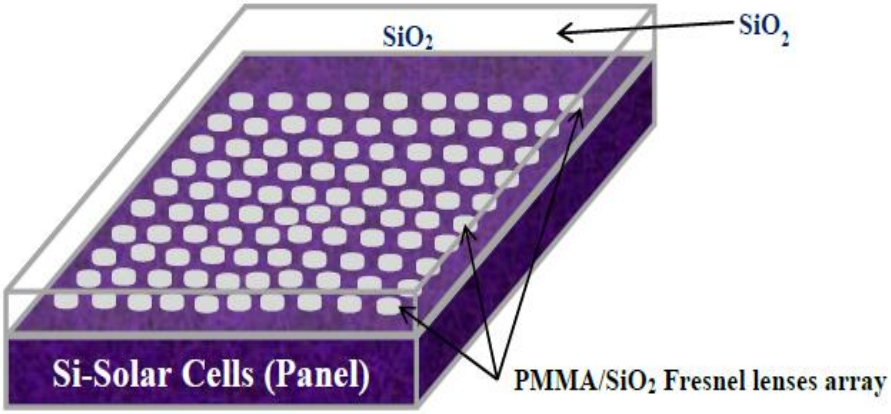

Fig. 3.1: Schematic illustration of PMMA/SiO_2 Fresnel lenses array on Silicon solar cells.

As depicted in Fig. 3.1, the basic idea is based on the concept of superposition. An array of micro Fresnel lenses converges the normally incident solar flux to the solar cell area. The micro array of Fresnel lenses CPV-system have a square shape consisting Fresnel lenses array expanding symmetrically from the optical centre. The dimensional parameters for the design of concentrating micro array of Fresnel lenses CPV-system are define in the following paragraphs:

Because of its optical sensitivity and wider applications in optical systems, the preliminary step of fabricating Fresnel lens is to design it. Therefore, to design a Fresnel lens, the fundamental parameters that determine the optical properties of the lens and mathematical relationship linking these parameters should be considered first. The parameters include; aperture size of the lens, wavelength, focal length, refractive index, among other (Davis, 2011). We now define the *relative aperture or f-number* in the following equation,

$$f - number = \frac{f}{D} \tag{3.01}$$

Where, f is the focal length, and D is the aperture diameter of the lens. Since Fresnel lens' structure composes of concentric circular rings at different depth, the

radius of the z^{th} ring r_z, can be expressed by the following equation (Tsui et al., 2012),

$$r_z = \sqrt{z\lambda f} \tag{3.02}$$

Where z is the number of Fresnel ring, f is the focal length, and λ is the wavelength. For an incident plane wave, the intensity distribution on the focal plane can be expressed by an Airy distribution function (Majumdar and Comtet, 2005), therefore if θ is the angle between the axis of the lens aperture and the line between lens' optical centre and eye piece, J_1 is the first order Bessel function and R is the lens' aperture radius. Then the intensity distribution I_θ is given by equation (3.03),

$$I_\theta \approx I_o \left| \frac{2J_1(kRsin\theta)}{kRsin\theta} \right|^2 \tag{3.03}$$

Where I_o is the maximum intensity of the Fresnel rings pattern at the lens' optical centre and *k* is the wavenumber. On the other hand, light passing through the lens bends, hence, the depth h at which the light (of wave number $k = \frac{2\pi}{\lambda}$) passed through a medium of refractive index n can be obtained by the equation, $knh - kh = 2\pi,$ which can further be simplify to obtained h as follows,

$$h = \frac{\lambda}{(n-1)} \tag{3.04}$$

The refractive index for a given medium of wavelength n_λ can be found by the Snell's law of refraction in the following equation,

$$n_\lambda = \frac{n_A sin\theta_i}{sin\theta_t} \tag{3.05}$$

Where θ_t is the refracted angle due to the medium and θ_i is incident angle due to air medium and $n_A = 1$ is the refractive index of air.

Depending on the material medium used, the refractive index n is almost constant for any given material medium, and is related to the wavelength λ by the Cauchy's equation,

$$n(\lambda) = A + B\lambda^{-2} + C\lambda^{-4} + \cdots \quad (3.06)$$

From equation (3.06), we have seen that as the wavelength λ increases, the latter polynomial terms decreases rapidly, thereby making the refractive index approaches a constant value. In plotting the relationship between the $n(\lambda)\ and\ \lambda$, the Cauchy's equations coefficients of different materials are different also. Furthermore, for micro-scale Fresnel lens fabricated by electron beam lithography (EBL) with the PMMA resist thickness h, the efficiency of generating i^{th} order $(i = \pm 1,\ \pm 2, \pm 3, \ldots\ldots\ldots)$ diffraction waves could be related to its diffraction efficiency. Then the diffraction efficiency η_i can be expressed as a (Teruo Fujita et al., 1981),

$$\eta_i = \frac{4}{i^2\pi^2} sin^2\left(\frac{\pi h(n-1)}{2\lambda cos\vartheta}\right) sin^2(n\pi\delta) \quad (3.07)$$

Where n is the refractive index of PMMA, λ is the wavelength of light, ϑ is the angle of incident light and δ is the duty ratio. On the other hand, for the same micro-scale Fresnel lens with a an asymmetric saw-tooth shape, the diffraction efficiency of m^{th} order diffraction waves can be expressed as (T Fujita et al., 1982),

$$\eta_m = [\frac{1}{T}\int_0^T e^{(i\varphi_{(x)})}\, e^{\left(-j\frac{2\pi mx}{T}\right)} dx]^2 \quad (3.08)$$

Where T is the grating period, $\varphi_{(x)}$ is the phase-retardation function of the grating and m is the diffraction order ($m = \pm 0, \pm 1, \pm 2, \pm 3 \ldots\ldots\ldots\ldots$).

In this work, the Fresnel rings were designed using GDSII Editor contained in Raith-ELPHY Quantum software explained in section 4.3 of chapter four. The designed Fresnel lens consists of eleven concentric circular rings expanding symmetrically from the optical centre. To minimize the reflection and simultaneously enhance the absorption and scattering of incident light on Si-solar cell, the diameter of the first Fresnel ring is chosen to be $\approx 5\,\mu m$, while the diameter of eleventh Fresnel ring been $\approx 52\,\mu m$. The relative aperture or $f-number$ was designed to be $\approx 1.26\,\mu m$ at the wavelength of $700\,nm$, and the thickness of each ring is assumed to be $\approx 500\,nm$ (which is smaller than wavelength of the band-gap energy of silicon). However, the focal length f_D varies with the variations of the wavelength λ. Table 3.1 shows the designed Fresnel lens parameters, Fig. 3.2 shows the plot of Fresnel rings radius against the Fresnel zone, while Fig. 3.3 shows the plot of the designed focal length against the wavelength.

Table 3.1: Designed parameters of Fresnel lens

Number of Fresnel Zone (Z)	Designed Radius R (μm)	$R^2(\mu m)^2$	Designed Diameter D (μm)	$D^2(\mu m)^2$
1	2.50	6.25	5.00	25.00
2	6.20	38.44	12.40	153.76
3	9.60	92.16	19.20	368.64
4	12.70	161.29	25.40	645.16
5	15.50	240.25	31.00	961.00
6	18.00	324.00	36.00	1296.00
7	20.20	408.04	40.40	1632.16
8	22.10	488.41	44.20	1953.64
9	23.70	561.69	47.40	2246.76
10	25.00	625.00	50.00	2500.00
11	26.00	676.00	52.00	2704.00

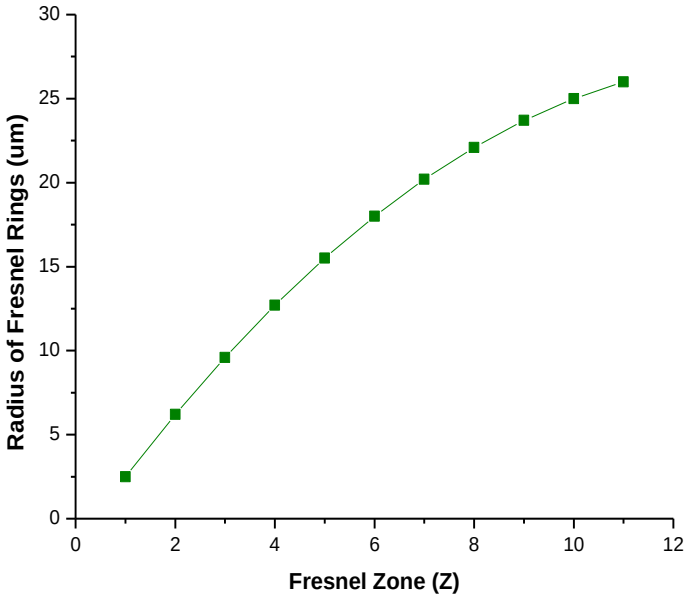

Fig. 3.2: Graphical representation of the designed Fresnel rings' radius against Fresnel zone Z.

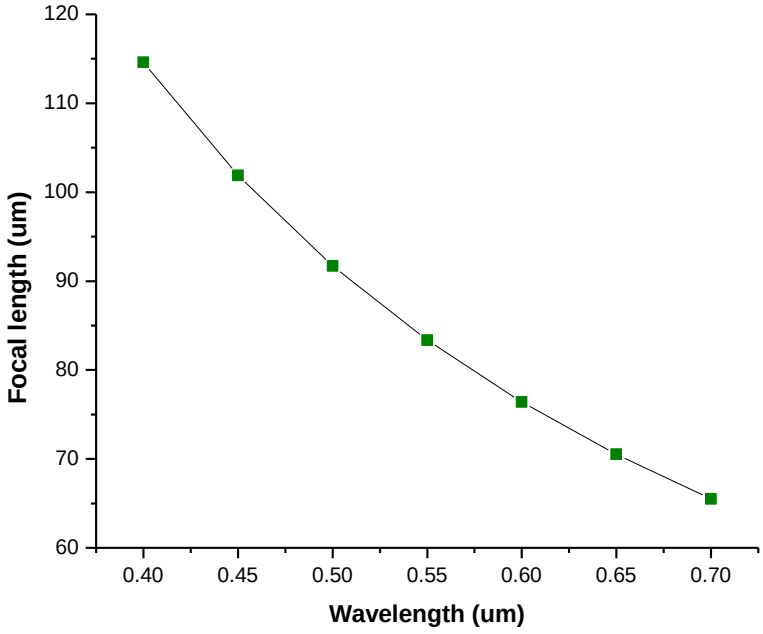

Fig. 3.3: The graphical relationship between the designed focal length of Fresnel lens and the wavelength of visible light.

3.2.1 Performance estimation of Fresnel lenses array CPV system

Generally, Fresnel lens used in concentrator photovoltaic applications are almost universally Plano-convex in which solar radiations are focused by means of a series of concentric grooves (also referred to as point focus) or parallel grooves (known as line focus). When parallel rays of light are passing through the aperture of the Fresnel lens, each ring of the prisms refracts the light at a slightly different angle and focuses on a focal point. Fig. 3.4 shows the schematic illustration of Fresnel lens.

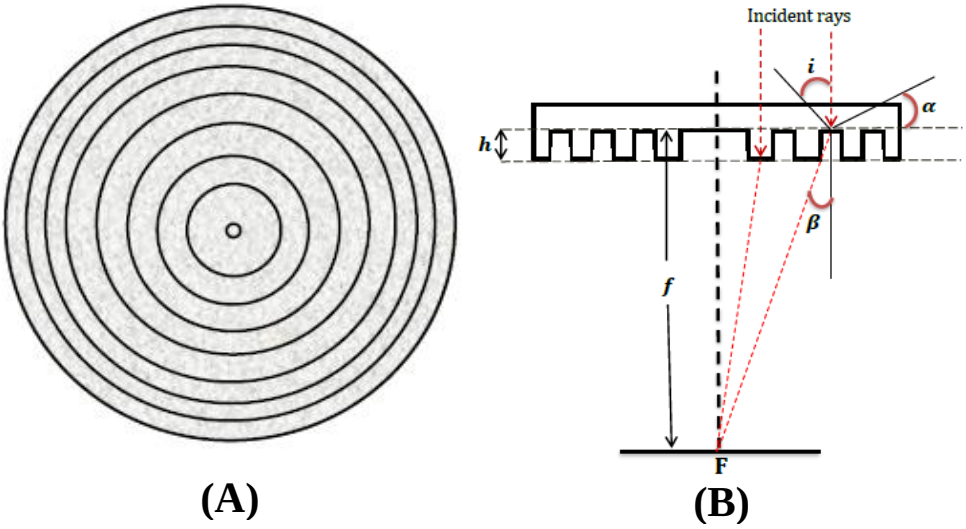

Fig. 3.4: Schematic illustration of Fresnel lens (a) 2-dimensional view showing the concentric rings of Fresnel lens (b) Side view showing the optical Parameters of binary Fresnel lens as a concentrator PV system.

From Fig. 3.4 (a), if the radius of outermost Fresnel ring is denoted as R_{Ext}, then the effective area A_{eff}, of this Fresnel lens is the sums of the increase in area due to formation of Fresnel rings can be obtain from following equation,

$$A_{eff} = A_{F-rings\,unit} + A_{\otimes} \qquad (3.09)$$